Electroosmotic Flow in Template-Prepared Carbon Nanotube Membranes

Scott A. Miller, Vaneica Y. Young, and Charles R. Martin*

Contribution from the Department of Chemistry, Center for Chemical Research at the Bio/Nano Interface, University of Florida, Gainesville, Florida 32611

Received August 9, 2001

Abstract: Carbon nanotube membranes (CNMs) were prepared by doing chemical vapor deposition of carbon within the pores of a microporous alumina template. Electroosmotic flow (EOF) was driven across the CNMs by allowing the membrane to separate two electrolyte solutions and using an electrode in each solution to pass a constant ionic current through the nanotubes. EOF was investigated by measuring the flux of a probe molecule (phenol) across the CNM. The as-synthesized CNMs have anionic surface charge, and EOF is in the direction of cation migration across the membrane. Measurements of the rate of EOF as a function of applied transmembrane current provided the ζ potential. The effect of pH on ζ provided the pK_a for the surface acidic sites responsible for this anionic charge; the acidic-site density was also determined. An electrochemical derivatization method was used to attach carboxylate groups to the nanotube walls; this enhances the anionic surface charge density, resulting in a corresponding increase in the EOF rate. Electrochemical derivatization was also used to attach cationic ammonium sites to the nanotube walls to yield CNMs that show EOF in the opposite direction of the as-synthesized or carboxylated membranes.

Introduction

Carbon nanotubes are of great current interest in both fundamental and applied science.[1−10] Potential applications for these tubular nanostructures include use in nanoelectronics,[1−4] hydrogen storage,[5,6] and battery[7,8] and field-emitting-display[9,10] technologies. We, and others, have shown that carbon nanotubes can be prepared via the template method[11−13] by doing chemical vapor deposition of carbon along the pore walls of microporous alumina membranes.[8,14−16] These membranes have cylindrical pores with monodisperse diameters, and a corresponding cylindrical nanotube is deposited within each pore. Carbon nanotubes with outside diameters as small as 20 nm have been prepared via this method.[16] Using an alternative template material and method, Joo et al. have prepared carbon nanotubes with outside diameters of 9 nm.[7]

At a recent workshop it was suggested that carbon nanotubes might be used as chemically selective filters.[17] This membrane-separation application will require alignment of the tubes[10,18−20] into a defect-free, mechanically strong membrane, where each tube spans the complete thickness of the membrane and the tube mouths are open at the faces of the membrane. While Sun and Crooks have recently developed an elegant procedure for doing this with a single carbon nanotube,[21] template synthesis inherently provides nanotube-containing membranes of this type, with up to 10^{11} nanotubes per cm^2 of membrane surface area.[13] Having large numbers of nanotubes per cm^2 of membrane area is essential to enhancing flux across the membrane, a critical issue in any membrane-separation processes.

Flux can also be enhanced by augmenting diffusive transport across the membrane with electrophoresis or with pressure-driven or electroosmotic flow. Sun and Crooks demonstrated diffusive, pressure driven, and electrophoretic transport of colloidal particles across their single carbon−nanotube membranes.[21] We describe here the first example of electroosmotic flow (EOF) in carbon nanotube membranes. EOF can be driven across the carbon nanotube membranes (CNMs) by allowing the membrane to separate two electrolyte solutions and using an electrode in each solution to pass a constant ionic current through the nanotubes. As per White et al., EOF was investi-

* Address correspondence to this author at crmartin@chem.ufl.edu.

(1) McEuen, P. L. *Nature* **1998**, *393*, 15−17.
(2) Tans, S. J.; Verschueren, A. R. M.; Dekker, C. *Nature* **1998**, *393*, 49−52.
(3) Ouyang, M.; Huang, J.-L.; Lieber, C. M. *Science* **2001**, *292*, 702−705.
(4) Rueckes, T.; Kim, K.; Joselevich, E.; Tseng, G. Y.; Cheung, C.-L.; Lieber, C. M. *Science* **2000**, *289*, 94−97.
(5) Liu, C.; Fan, Y. Y.; Cong, H. T.; Cheng, H. M.; Dresselhaus, M. S. *Science* **1999**, *286*, 1127−1129.
(6) Chen, P.; Wu, X.; Lin, J.; Tan, K. L. *Science* **1999**, *285*, 91−93.
(7) Joo, S. H.; Choi, S. J.; Oh, I.; Kwak, J.; Liu, Z.; Terasaki, O.; Ryoo, R. *Nature* **2001**, *412*, 169−172.
(8) Che, G.; Lakshmi, B. B.; Fisher, E. R.; Martin, C. R. *Nature* **1998**, *393*, 346−349.
(9) de Heer, W. A.; Châtelain, A.; Ugarte, D. *Science* **1995**, *270*, 1178−1180.
(10) Fan, S.; Chapline, M. G.; Franklin, N. R.; Tombler, T. W.; Cassell, A. M.; Dai, H. *Science* **1999**, *283*, 512−515.
(11) Martin, C. R.; Mitchell, D. T. *Anal. Chem.* **1998**, *70*, 322A-327A.
(12) Hulteen, J. C.; Martin, C. R. *J. Mater. Chem.* **1997**, *7*, 1075−1087.
(13) Martin, C. R. *Science* **1994**, *266*, 1961−1966.
(14) Che, G.; Miller, S. A.; Fisher, E. R.; Martin, C. R. *Anal. Chem.* **1999**, *71*, 3187−3191.
(15) Che, G.; Lakshmi, B. B.; Martin, C. R.; Fisher, E. R. *Langmuir* **1999**, *15*, 750−758.
(16) Kyotani, T.; Tsai, L. F.; Tomita, A. *Chem. Commun.* **1997**, *7*, 701−702.
(17) Baum, R. M. *Chem. Eng. News* **1997**, *June 30*, 39−41.
(18) Schlittler, R. R.; Seo, J. W.; Gimzeski, J. K.; Durkan, C.; Saifullah, M. S. M.; Welland, M. E. *Science* **2001**, *292*, 1136−1139.
(19) Li, W. Z.; Xie, S. S.; Qian, L. X.; Chang, B. H.; Zou, B. S.; Zhou, W. Y.; Zhao, R. A.; Wang, G. *Science* **1996**, *274*, 1701−1703.
(20) Ren, Z. F.; Huang, Z. P.; Xu, J. W.; Wang, J. H.; Bush, P.; Siegal, M. P.; Provencio, P. N. *Science* **1998**, *282*, 1105−1107.
(21) Sun, L.; Crooks, R. M. *J. Electrochem. Soc.* **2000**, *122*, 12340−12345.

10.1021/ja011926p CCC: $20.00
Published on Web 11/10/2001

gated by measuring the flux of a probe molecule across the membrane.[22,23] The as-synthesized CNMs have anionic surface charge, and as a result, EOF is in the direction of cation migration across the membrane. An electrochemical derivatization method was used to attach carboxylate groups to the nanotube walls;[24−26] this enhances the anionic surface charge density, resulting in a corresponding increase in the EOF rate. Electrochemical derivatization can also be used to attach cationic ammonium sites to the nanotube walls to yield CNMs that show EOF in the opposite direction of the as-synthesized or carboxylated membranes.

Experimental Section

Materials. Whatman Anodisc microporous alumina filters were used as the template membranes. Argon, nitrogen, phenol, $AgNO_3$, *p*-aminobenzoic acid, and 2-(4-aminophenyl)ethylamine were used as received. A 30:70 (v/v) mixture of ethylene and He was used for CVD of the carbon nanotubes. Absolute ethanol was dried over 3A molecular sieves. $LiClO_4$ was dried at 90 °C. Purified water was prepared by passing house-distilled water through a Millipore Milli Q water purification system. Buffer solutions were prepared from monobasic sodium phosphate and adjusted to pH 7.2 with 1 M NaOH.

Preparation of the Carbon Nanotube Membranes (CNMs). The CVD method used has been described previously.[8,14,15] Briefly, prior to CVD synthesis, the alumina template membranes were pressed between two quartz plates and heated to 740 °C for 1 h. If this heat pretreatment is not done, the alumina membranes curl into a tight cylinder during the CVD synthesis of the carbon nanotubes. Heat pretreatment between quartz plates prevents this unwanted curling, and allows for synthesis of planar CNMs.

The CVD reactor consisted of a quartz tube (diameter = 4.2 cm, length = 52 cm) that was placed within a tube furnace. A 3.5 × 1.5 cm semicircle of the heat-treated alumina template membrane was placed vertically in the CVD reactor and the reactor temperature was increased to 670 °C, under argon flow. When the temperature stabilized, the Ar flow was terminated, and simultaneously a 20-cm^2 flow of ethylene gas mixture was initiated. Under these conditions ethylene pyrolyzes to yield carbon nanotubes on the pore walls as well as thin carbon films on both faces of the membrane. Deposition was continued for 5.5 h after which the Ar flow was resumed, the ethylene flow was terminated, and the furnace was turned off and allowed to cool to room temperature. After synthesis the membranes were stored in air for at least 24 h prior to use. This results in oxidation of the carbon surfaces to yield acidic surface sites on the nanotube walls.[27−29] CNMs treated in this way are referred to as "as-synthesized" membranes. Four different membranes were used for these studies; the success rate for preparing these membranes approaches 100%.

X-ray Photoelectron Spectroscopy (XPS). XPS studies of the samples were performed on a Kratos XSAM 800 spectrometer with Mg Kα excitation (200 W). The samples were mounted onto a stainless steel sample stub by means of a 7 mm diameter carbon sheet disk (SPI Supplies), so as to completely cover both the carbon disk and the sample stub. The samples were inserted into the sample analyzer chamber by means of a quick insertion probe, and spectral acquisition with the fixed analyzer transmission mode commenced after the pressure decreased to 5×10^{-9} Torr. Survey scans, high-resolution C 1s spectra, and high-resolution O 1s spectra were recorded at a takeoff angle of 20° relative to the sample surface. The information depth (99% criterion, calculated as 3D, where D is the mean escape depth) [30] is estimated as 2.5 nm for C 1s. Data analysis was done by using the DS 800 software package. Peak positions were all referenced to 285.0 eV for the main carbon peak.

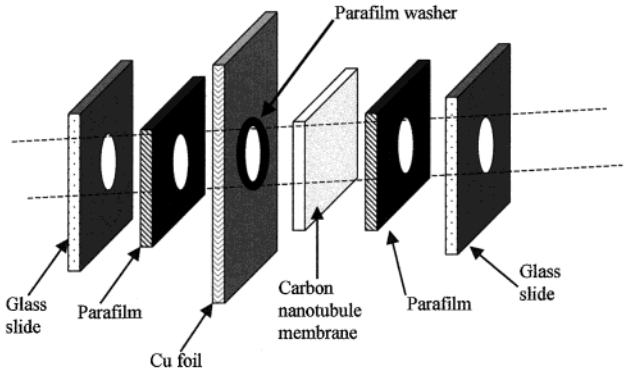

Figure 1. Exploded view of the nanotube membrane assembly. The holes in glass slides and Parafilm are 0.95 cm across. The hole in the Cu foil is 1.27 cm across.

Permeation Measurements. The CNM was mounted in the supporting assembly shown in Figure 1. After assembling the various components, the assembly was heated for 3 min at 150 °C in an oven to melt the Parafilm, which acted as a glue to hold the various pieces together. This assembly exposes a 0.713-cm^2 portion of the CNM to the electrolyte solution. The assembly also allows electrical contact to be made to the membrane so that it can be used as the working electrode for the electrochemical derivatizations. Electroosmotic flow (EOF) measurements were made in a simple U-tube permeation cell.[31] The membrane assembly was clamped between the two halves of the U-tube cell and both half-cells were filled with 25 mL of pH 7.2 phosphate buffer. Unless otherwise stated, the ionic strength of the buffer was 0.01 M. The resistivities of the electrolyte solutions used were determined by using an Accumet AR-50 conductivity meter.

An EG&G 173 galvanostat was used to pass a constant ionic current through the CNM. This current was responsible for EOF in the membrane. The rate and direction of EOF was varied by varying the magnitude and sign of the applied current. The faradaic reactions occurring at the Pt electrodes (that support the ionic current in the nanotubes) were simply the reduction and oxidation of water. The alternative to this constant current approach would be to apply a constant transmembrane potential. However, in this case, the voltage drop across the membrane would have to be independently determined.

The feed half-cell was 4.82 mM in the small, electrically neutral, chromophoric probe phenol. As per Bath et al.,[22,23] the rate of EOF was determined by monitoring the transport of the probe molecule across the membrane and into the permeate half-cell. This was accomplished by continuously pumping the permeate solution through a Waters 486 HPLC UV/visible detector set at 270 nm. An Eldex Laboratories AA-100-S piston pump was used to circulate permeate solution through the detector. Absorbance data were obtained at a rate of 20 points per minute. These data were logged on a PC that was interfaced to the absorbance detector. The absorbance data were converted to moles of phenol transported with the aid of a calibration curve. These data were processed as plots of micromoles of phenol transported vs time. These plots appear as uninterrupted lines because of the large quantity of data obtained.

The following sign convention was employed: For a positive applied current, the anode was in the feed half-cell and the cathode was in the permeate half-cell. In this case, cations migrated from feed to permeate and anions from permeate to feed. A negative applied current had the opposite configuration, i.e., cathode in the feed half-cell and anode in

(22) Bath, B. D.; Lee, R. D.; White, H. S.; Scott, E. R. *Anal. Chem.* **1998**, *70*, 1047−1058.
(23) Bath, B. D.; White, H. S.; Scott, E. R. *Anal. Chem.* **2000**, *72*, 433−442.
(24) Barbier, B.; Pinson, J.; Desarmot, G.; Sanchez, M. *J. Electrochem. Soc.* **1990**, *137*, 1757−1764.
(25) Deinhammer, R. S.; Ho, M.; Anderegg, J. W.; Porter, M. D. *Langmuir* **1994**, *10*, 1306−1313.
(26) Liu, J.; Cheng, L.; Liu, B.; Dong, S. *Langmuir* **2000**, *16*, 7471−7476.
(27) Panzer, R. E.; Elving, P. J. *Electrochim. Acta* **1975**, *20*, 635−647.
(28) Bismarck, A.; Springer, J. *Colloids Surf. A: Physicochem. Eng. Asp.* **1999**, *159*, 331−339.
(29) Garcia, A. B.; Cuesta, A.; Montes-Moran, M. A.; Martinez-Alonso, A.; Tascon, J. M. D. *J. Colloid Interface Sci.* **1997**, *192*, 363−367.
(30) Powell, C. J.; Jablonski, A.; Tilinin, I. S.; Tanuma, S.; Penn, D. R. *J. Electron Spectrosc. Relat. Phenom.* **1999**, *98*−*99*, 1−15.
(31) Jirage, K. B.; Hulteen, J. C.; Martin, C. R. *Anal. Chem.* **1999**, *71*, 4913−4918.

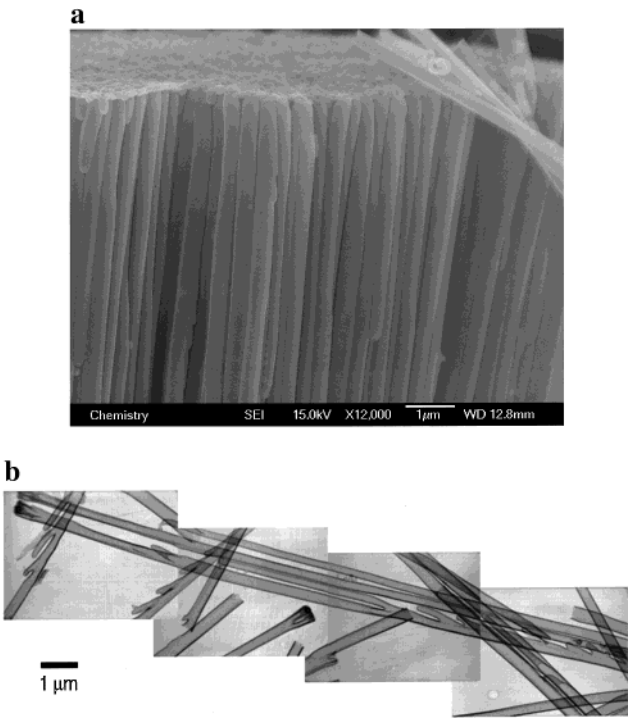

Figure 2. (A) SEM image of a CNM cross-section after removal of the alumina template. (B) TEM image montage of individual carbon nanotubes removed from a CNM.

the permeate half-cell. The current values are reported here as the current density, defined as the applied current divided by the total pore area of the membrane. The total pore area was determined from the known diffusion coefficient for phenol in water at 298 K (9.68×10^{-6} cm^2 s^{-1}),[32] the known concentration gradient of phenol across the membrane, and the measured diffusive flux (no applied current) of phenol across the membrane.

Electrochemical Derivatization of the Carbon Nanotubes. An electrochemical derivatization scheme[24−26] was used to attach carboxylate groups to the nanotube walls. This method entails the electrooxidation of *p*-aminobenzoic acid (PABA) to a cation radical at the carbon nanotube walls. This results in the formation of a C−N bond, thus covalently attaching PABA to the tube walls. Dong et al. used a series of electrochemical experiments at glassy carbon electrodes to prove that at neutral pH values, the PABA dissociates to yield covalently bound surface carboxylate groups.[26] A similar approach was used to attach positively charged ammonium sites to the nanotube walls. This entailed electrochemical oxidation of 2-(4-aminophenyl)ethylamine (APEA) at the carbon nanotube membrane to yield covalently bound APEA. At neutral pH values the free (not bound to the tube wall) amine sites are protonated to the corresponding ammonium.

The electrochemical cell used for these derivatizations consisted of the CNM working electrode, a Ag/Ag^+ reference electrode (0.01 M $AgNO_3$ in anhydrous ethanol), and a platinum mesh counter electrode; the electrolyte solution was 0.1 M $LiClO_4$ in anhydrous ethanol which was also 3 mM in either PABA [26] or APEA. The electrochemical reaction was carried out by scanning the potential of the carbon nanotube membrane working electrode three times between 0 and +1.2 V vs Ag/Ag^+ (scan rate = 10 mV s^{-1}).

Electron Microscopy. Scanning electron microscopy (SEM) and transmission electron microscopy (TEM) were used to image the carbon nanotubes prepared within the pores of the alumina template membrane. This was accomplished by first dissolving away the alumina by immersion (for 12 h) in 49% HF. The HF was removed by pipet leaving the liberated nanotubes (connected together by the carbon surface films, Figure 2A), which were rinsed with methanol and then suspended in methanol. This suspension was then ultrasonicated for 20 min. It is important to point out that removal of the template membrane in this way was only done for the SEM and TEM images. All permeation studies were done with the carbon nanotubes still embedded within the pores of the alumina template.

For the preparation of SEM samples a drop of the ultrasonicated membrane suspension was applied to a copper foil adhered to a SEM stub and the solvent was allowed to evaporate. Gold was sputtered onto the sample to improve electrical conductivity. Images were obtained by using a JEOL 6335F field emission gun microscope. For TEM imaging a drop of the suspension was applied to a Carbon Type A TEM grid. The carbon nanotubes adhered well to the grid and were easily imaged with use of a JEOL 2000 microscope.

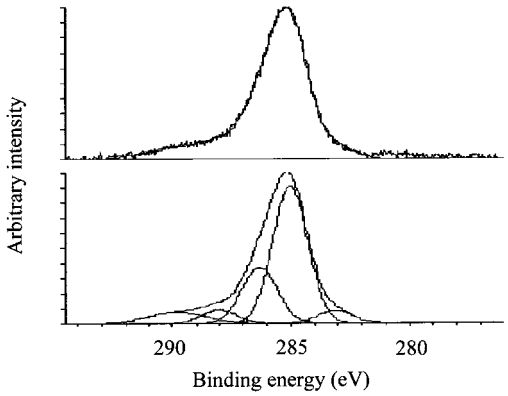

Figure 3. High-resolution C 1s spectrum showing the experimental spectrum, the fitted envelope, and the individual peaks for the fit.

Results and Discussion

Electron Microscopy. Figure 2A shows a cross-sectional image of the CVD carbon nanotubes after dissolution of the alumina template. A parallel array of nanotubes is obtained because the tubes are connected together by the carbon surface film that can be seen at the top of the image. While it is not evident from this image, this carbon surface film does not block the mouths of the nanotubes. The outside diameter of the nanotubes (∼300 nm) is larger than the nominal pore diameter of the template. Our SEM and TEM images indicate that this is because the pores are, in fact, larger than the nominal diameter for most of the thickness of the membrane but branch at one face of the membrane into smaller (diameter ∼200 nm) pores. This branching can be seen in the TEM image shown in Figure 2B. Branching undoubtedly results from the voltage reduction technique used during the final step of the electrochemical process used to prepare these alumina membranes.[33]

Figure 2B shows a TEM montage image of individual carbon nanotubes that had become separated from the carbon surface films during ultrasonication of the nanotube suspension. The branched ends of the nanotubes discussed above are clearly seen in this image. This image also shows that the tubes have a consistent wall thickness down their entire length; a wall thickness value of ∼40 nm was obtained from such images.

XPS. Survey scans (not shown) indicate that only oxygen and carbon are present on the surface of the CNMs. While these spectra were obtained with the underlying alumina membrane still intact, there is no observable signal for Al because the carbon layer is too thick (∼40 nm). This allows us to assign the oxygen signal to oxygen-containing functional groups on the carbon surface. The high-resolution C 1s spectra may be fitted to five peaks (Figure 3). The top panel of Figure 3 shows the fit envelope overlaid on the original spectrum; the bottom panel shows the peak contributions to the fitted envelope. The

(32) Yaws, C. L.; Nijhawan, S.; Li, K. Y. In *Handbook of Transport Property Data: Viscosity, Thermal Conductivity, and Diffusion Coefficients of Liquids and Gases*; Yaws, C. L., Ed.; Gulf Pub. Co.: Houston, TX, 1995.

(33) Hornyak, G. L.; Patrissi, C. J.; Martin, C. R. *J. Phys. Chem.* **1997**, *101*, 1548−1555.

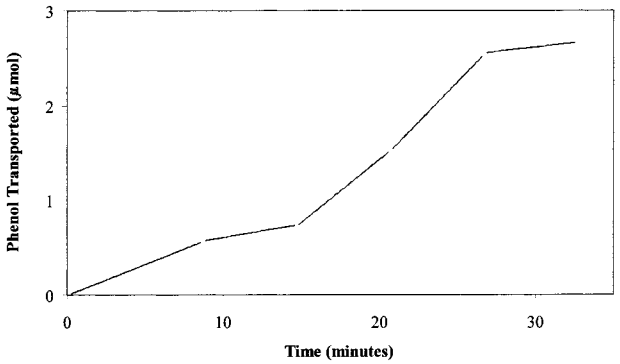

Figure 4. Micromoles of phenol transported vs time at various values of applied current density (see text for current density values).

Table 1. Effect of Applied Current Density on the Flux, Enhancement Factor, and Electroosmotic Velocity in the Carbon Nanotubule Membrane

J_{app}, mA/cm^2	Flux, nmol/(min·cm^2)[a]	E	v_{eo}, μm/s
−10.1	25.8	0.280	−35.0
−7.2	39.3	0.426	−24.5
0.00	92.1	1.000	0.0
+7.2	187.1	2.030	26.3
+10.1	237.9	2.581	37.6

[a] The geometric area of the membrane (0.713 cm^2) was used.

binding energies for the five peaks are as follows: 283.9 ± 0.4, 285.0 (reference peak), 286.3 ± 0.5, 287.8 ± 0.5, and 289.9 ± 0.4 eV, where the averages are for 6 values, and the uncertainties are the unbiased standard deviations.

Ramm et al. have recently used XPS to characterize the surface composition of plasma-deposited amorphous carbon films.[34] They assign the two lowest binding-energy peaks to graphitic (284 eV) and amorphous (285 eV) carbon present at the surface of the sample. The predominance of the 285 eV peak indicates that, in agreement with prior results, these carbon nanotubes are amorphous.[35] They can, however, be converted to highly ordered graphite via a Ni catalysis method.[35] The three higher binding-energy peaks are due to oxygen-containing surface functional groups. These three peaks may be assigned as follows: 286.3 ± 0.5 eV (alcohol or phenolic hydroxyl, ether); 287.8 ± 0.5 eV (aldehyde, ketone); and 289.9 ± 0.4 eV (carboxylic acid, ester, carboxylic acid anhydride).[36] It is well-known that air-oxidized carbon surfaces contain carboxylic acid groups,[27−29] and presumably anhydride would hydrolyze to the acid upon exposure to water. These sites contribute to the intensity of the 289.9 eV peak. However, XPS alone cannot distinguish between −COOH and the contribution from ester sites. As we will see, EOF measurements allow for a determination of both the surface density of acidic sites and the surface pK_a.

Effect of Magnitude of the Applied Current on Permeate (Phenol) Flux. Figure 4 shows a plot of micromoles of phenol transported across the carbon nanotube membrane at various values of applied current density. This plot consists of five linear segments, and the slope of each segment is the flux of phenol (N_J) at that applied current density (Table 1). The first linear segment in Figure 4 (0 to 8.5 min) was obtained with no applied current, and the flux in this case is simply the diffusive flux of phenol, N_{diff}, from the feed across the membrane and into the permeate. The second linear segment (9 to 14.5 min) was obtained with an applied current density, $J_{app} = -7.2$ mA cm^{-2}. The flux of phenol across the membrane was observed to decrease, indicating EOF in the opposite direction of the diffusive flux (EOF from permeate solution to feed solution). This is confirmed by data in the third linear segment (15 to 20.5 min), which were obtained with $J_{app} = +7.2$ mA cm^{-2}; now the net flux is higher than the diffusive flux (Table 1), indicating EOF in the direction of diffusive transport. The final two linear segments were obtained at higher positive and negative applied current densities, and further enhancement and diminution, respectively, in the flux is observed.

Calculation of the Electroosmotic Velocity. In the presence of the applied transmembrane current, the steady-state flux of permeant across a membrane is described by the Nernst−Plank equation[37]

$$N_J = -D[\delta C(x)/\delta x] - zF(RT)^{-1}DC[\delta\phi(x)/\delta x] \pm Cv_{eo} \quad (1)$$

where D, C, and z are the diffusion coefficient, concentration, and charge of the permeate molecule, respectively, $\delta C(x)/\delta x$ is the concentration gradient in the x direction across the membrane, $\delta\phi(x)/\delta x$ is the potential gradient in the electrolyte within the nanotubes, and v_{eo} is the electroosmotic velocity. The three terms in eq 1 describe the diffusive, migrational, and EOF-convective transport processes, respectively. Because phenol is a neutral molecule at the pH used here, eq 1 simplifies to

$$N_J = -D[\delta C(x)/\delta x] + Cv_{eo} \quad (2)$$

When $J_{app} = 0$, only the first term in eq 2 is operative and the flux is the diffusive flux, N_{diff}.

The experimental flux data in Table 1 can be used to calculate a parameter called the enhancement factor, E, which can then be used to calculate the electroosmotic velocity.[37] E is given by,

$$E = N_J/N_{diff} \quad (3)$$

i.e., the ratio of the flux in the presence of an applied current to the flux at $J_{app} = 0$. E values for the data in Figure 4 are presented in Table 1. When a positive current is applied, E is greater than unity, indicating, again, EOF in the direction of the diffusional flux. Analogous results were obtained by Bath et al. for Nafion membranes, where EOF is due to the polymer's fixed sulfonate sites.[22] This indicates that as would be expected for air-treated carbon, the pore walls on the carbon nanotubes have fixed negatively charged sites.[27−29]

Following Srinivasan and Higuchi, [37] the peclet number (Pe) can be calculated from E via

$$E = \mathrm{Pe}/(1 - (\exp(-\mathrm{Pe})) \quad (4)$$

Pe can then be used to calculate v_{eo} using[37]

$$v_{eo} = \mathrm{Pe}\ D/l \quad (5)$$

where l is the thickness of the membrane. Because the inside diameter of the carbon nanotubes (∼120 nm) is ∼500 times larger than the diameter of phenol, hindered diffusion[38] does not occur in these tubes, and the bulk solution diffusion coefficient can be used in eq 5. This and the membrane thickness

(34) Ramm, M.; Ata, A.; Brzezinka, K.-W.; Gross, T.; Unger, W. *Thin Solid Films* **1999**, *354*, 106−110.
(35) Che, G.; Lakshmi, B. B.; Martin, C. R.; Fisher, E. R.; Ruoff, R. S. *Chem. Mater.* **1998**, *10*, 260−267.
(36) Beamson, G.; Briggs, D. *High-Resolution XPS of Organic Polymers: The Scienta ESCA 300 Database*; Wiley: Chichester, England, 1992.
(37) Srinivasan, V.; Higuchi, W. I. *Int. J. Pharm.* **1990**, *60*, 133−138.
(38) Renkin, E. M. *J. Gen. Physiol.* **1954**, *38*, 225.

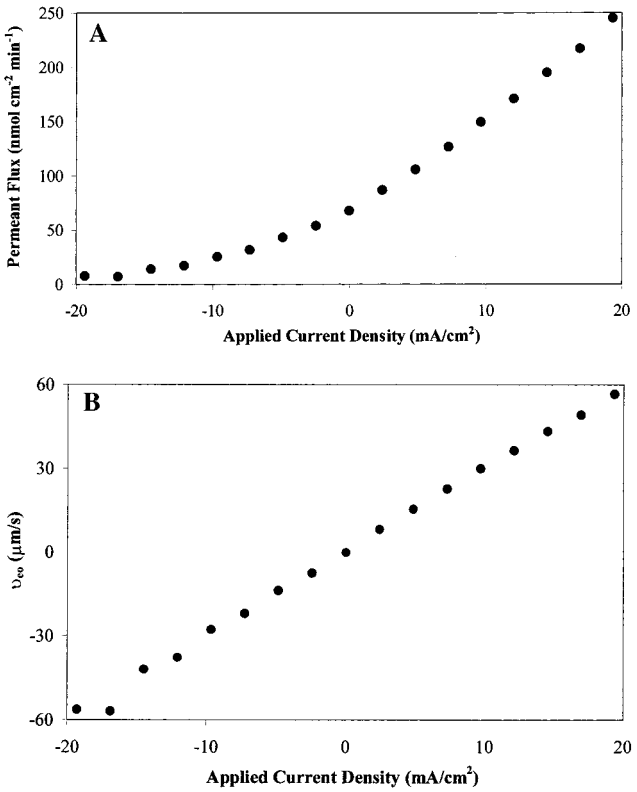

Figure 5. (A) Plot of phenol flux vs applied current density. (B) Plot of electroosmotic flow velocity vs applied current density.

(0.006 cm) give the v_{eo} data shown in the last column in Table 1. As would be expected, current densities of the same magnitude but opposite sign give v_{eo} values of approximately the same magnitude but opposite sign.

Effect of Applied Current Density on v_{eo}. Phenol transport data like those shown in Figure 4 were obtained for 16 different J_{app} values between +19.3 and −19.3 mA cm^{-2}. Figure 5A shows the corresponding flux vs J_{app} data. As would be expected from the above results, flux increases with J_{app} for positive currents, indicating the increasing importance of EOF to the transport of permeate across the membrane. At sufficiently negative J_{app} values, the net flux asymptotically approaches zero. In this case, EOF from the permeate half-cell to the feed half-cell is negating the diffusive flux from feed to permeate.[22]

The Helmholtz−Smoluchowski equation[39] describes the relationship between the electroosmotic velocity and the linear electric field gradient ($E(x)$, V cm^{-1}) across the membrane

$$v_{eo} = -\epsilon\zeta E(x)/\eta \qquad (6)$$

where ϵ and η are the permittivity and viscosity of the solution within the nanotubes, respectively, and ζ is the ζ-potential of the tube walls. Substituting the product of the applied current density and the resistivity of the electrolyte within the nanotubes, ρ, for the $E(x)$ in eq 6 gives

$$v_{eo} = -\epsilon\zeta J_{app}\rho/\eta \qquad (7)$$

which shows that v_{eo} is linearly related to the applied current density. Equations 4 and 5 were used to calculate v_{eo} from the flux data in Figure 5A. Figure 5B shows a plot of v_{eo} vs current density; in agreement with eq 7, a linear relationship is obtained. (Some deviation is observed at the highest negative J_{app} values.

(39) Probstein, R. F. *Physicochemical Hydrodynamics*; Buttersworth: Stoneham, MA, 1989.

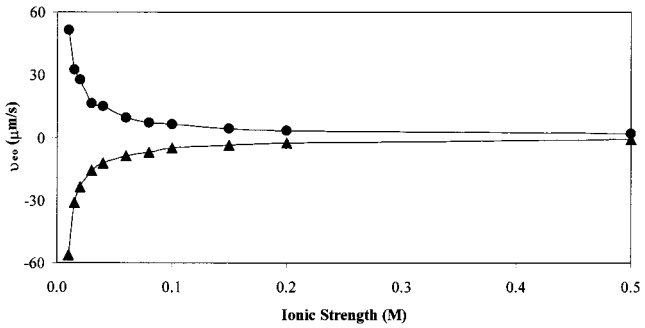

Figure 6. Plots of electroosmotic flow velocity vs the ionic strength of the permeate and feed solutions. Applied current densities were (▲) −19.7 and (●) +19.7 mA cm^{-2}.

This is because the flux is nearly zero at such large negative J_{app} values, making the error in the measurement large.)

According to eq 7, the slope of the v_{eo} vs J_{app} plot in Figure 5b is $-\epsilon\zeta\rho/\eta$. Using the known values for the permittivity and viscosity of water (6.95×10^{-10} C^2 J^{-1} m^{-1} and 0.890 cP, respectively [40]) and the measured resistivity of the electrolyte (2.23 kΩ cm), the slope can be used to calculate the ζ-potential for the CNM. A value of $\zeta = -17.3$ mV was obtained from these data. Bismark et al. obtained similar ζ-potential values for carbon fibers,[28] and Garcia et al. obtained somewhat larger ζ-potential values (~ -45 mV) after grinding such carbon fibers.[29]

It should be noted that eqs 6 and 7 are based on the assumption that the thickness of the double layer at the pore wall is much smaller than the pore radius. Because the double layer at this electrolyte concentration is less than 3 nm in thickness,[39] this is clearly a valid assumption. Finally, for this reason and because the measured ζ-potential is relatively low, deviations due to surface conductance, or changes in the permittivity, and viscosity within the nanotubes are negligible.[41,42] Thus, it is reasonable to use the resistivity, permittivity, and viscosity of the bulk solution in the ζ-potential calculation.

Effect of Ionic Strength of the Electrolyte on v_{eo}. Phenol transport data were obtained at applied current densities of +19.7 and −19.7 mA cm^{-2} in solutions with ionic strength varying from 0.01 to 0.50 M (Figure 6). The pH of the electrolyte was maintained at 7.2. Transport data for the case $J_{app} = 0$ were also obtained over this electrolyte concentration range. No change in the diffusional flux was observed (<3% relative standard deviation), indicating that the diffusion coefficient for phenol does not vary with electrolyte concentration over this concentration range. Figure 6 shows plots of v_{eo} vs ionic strength obtained from the transport data. The general trend—that the absolute value of v_{eo} decreases with increasing ionic strength—is expected.

Returning to eq 7, we see that v_{eo} is directly proportional to the ζ-potential, which is related to the Debye length, κ^{-1} (the effective thickness of the electrical double layer), by [43]

$$\zeta = 2kT/ze \sinh^{-1}(\sigma\kappa^{-1}ze/(2\epsilon kT)) \qquad (8)$$

where k is the Boltzmann constant, T is temperature, e is the elementary charge, and σ is the surface charge density at the plane of shear between the nanotube wall and the electrolyte.

(40) Weast, R. C.; Astle, M. J.; Beyer, W. H., Eds. *CRC Handbook of Chemistry and Physics*, 66th ed.; CRC Press, Inc.: Boca Raton, FL, 1985.
(41) Rice, C. L.; Whitehead, R. *J. Phys. Chem.* **1965**, *69*, 4024.
(42) Levine, S.; Marriott, J. R.; Neale, G.; Epstein, N. *J. Colloid Interface Sci.* **1975**, *52*, 136−149.
(43) Jimbo, T.; Tanioka, A.; Minoura, N. *Langmuir* **1998**, *14*, 7112−7118.

For the ζ-potential and Debye length ranges investigated here eq 8 simplifies to

$$\zeta = \sigma\kappa^{-1}/\epsilon \tag{9}$$

For a symmetrical electrolyte, κ^{-1} is related to the concentration of the electrolyte via[39]

$$\kappa^{-1} = (9.61 \times 10^{-9})(z^2c)^{-1/2} \tag{10}$$

Equation 10 shows that the double layer thickness decreases with increasing ionic strength of the electrolyte, which means that the ζ-potential decreases with increasing ionic strength (eq 9). This, in turn, causes $|v_{eo}|$ to decrease with increasing ionic strength (eq 7), which is the experimentally observed trend in Figure 6.

A second factor contributes to the observed decrease in $|v_{eo}|$ with increasing ionic strength. Equation 7 shows that v_{eo} is also proportional to the resistivity of the electrolyte, ρ, which of course is inversely proportional to the number of charge-carrying ions in the solution. Hence, ρ decreases with increasing ionic strength of the electrolyte, and eq 7 predicts that this would also contribute to the observed decrease in v_{eo} with increasing ionic strength (Figure 6).

If it is assumed that κ^{-1} decreases with ionic strength (μ) as $\kappa^{-1} \propto \mu^{-1/2}$ (eq 10) and that ρ decreases with μ as $\rho \propto \mu^{-1}$, we would predict that v_{eo} would decrease with μ via $v_{eo} \propto \mu^{-3/2}$. The experimental data (Figure 6) were fit to the relationships $v_{eo} \propto \mu^{-0.9}$ ($R^2 = 0.993$) for the positive current density and $v_{eo} \propto -\mu^{-1.0}$ ($R^2 = 0.997$) for the negative current density. Hence, the experimental falloff of v_{eo} with increasing μ is less than the predicted value.

Another factor needs to be considered. As shown in eq 9, the ζ-potential is also directly proportional to the charge density. The charge density can be divided into two general categories: covalently bound charge and adsorbed charge. We discuss the effect of the quantity of covalently bound charge on v_{eo} in the following section. It is possible that over the very large ionic strength range investigated in Figure 6, there is a significant change in the quantity of adsorbed charge from the electrolyte. Adsorbed charge would primarily come from the anions of the electrolyte, and this adsorbed negative charge would increase with increasing μ. This would cause both the ζ-potential and v_{eo} to increase with increasing μ. Since this is the opposite trend as the $\kappa^{-1} \propto \mu^{-1/2}$ and the $\rho \propto \mu^{-1}$ dependences discussed above, this would make the net decrease in v_{eo} with increasing μ less extreme than the predicted $\mu^{-3/2}$ dependence, and this is what is observed experimentally.

Finally, at the highest ionic strength used in Figure 6, both the negative and positive electroosmotic velocities decrease nearly to zero. This shows that the effect of double layer compression on the ζ-potential (that causes v_{eo} to decrease with increasing ionic strength) dominates any effect of increasing adsorbed negative charge at high ionic strengths.

Effect of Solution pH on v_{eo}. Phenol transport data were obtained at applied current densities of positive and negative 24.9 mA cm^{-2} from solutions that were 10 mM in NaCl and 0.5 mM in phosphate, with the pH adjusted to values between 3 and 8. The NaCl served to maintain the ionic strength at a constant value. The v_{eo} vs solution pH data are shown in Figure 7A. In general, the expected trend for surface acidic sites is observed, i.e., v_{eo} is high at high pH values, where the sites are deprotonated, and goes to zero at lower pH values, where the sites are protonated. There are, however, two features of the data in Figure 7A that are unexpected.

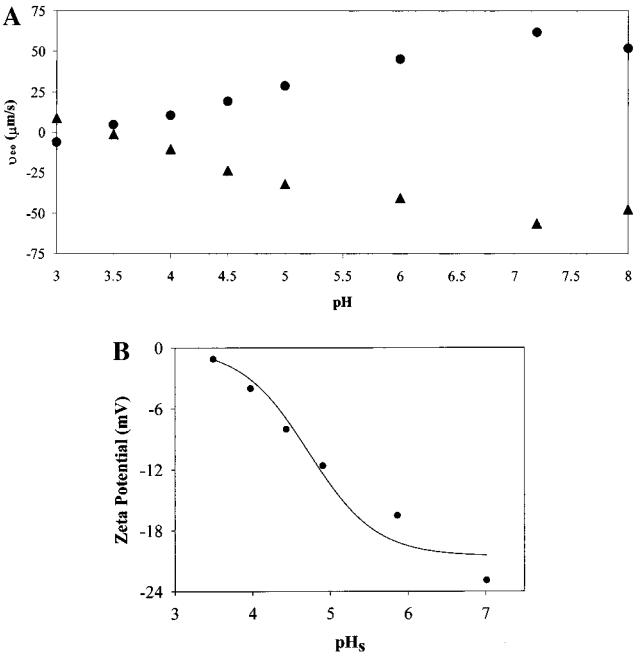

Figure 7. (A) Plots of electroosmotic flow velocity vs pH. Applied current densities were (▲) −24.9 and (●) +24.9 mA cm^{-2}. (B) Plot of ζ potential of the CNM vs surface pH (eq 11). The points are the experimental data and the curve is the best fit to eq 13.

First, while v_{eo} goes to zero at pH ∼3.5, at lower pH the flow resumes again, but in the opposite direction. This indicates that positive sites are introduced by protonation of some very weakly basic surface functional group. Such protonatable carbon sites have been known for some time and have been attributed to two chemical features of the carbon:[44] pyrone-like structures and basal-plane sites that act as Lewis bases. These protonatable carbon sites have also been observed in ζ-potential measurements of carbon fibers.[28,29] The presence of these sites makes the EOF characteristics of the carbon nanotubes quite interesting because the direction of EOF can be switched by controlling the pH of the contacting solution phase.

The second unexpected feature of the data in Figure 7A is that $|v_{eo}|$ is lower at pH 8.0 than at pH 7.2. While it is tempting to attribute this to experimental error, it was observed at all current densities studied and with both positive and negative currents. This is unexpected because the fraction of the deprotonated form of a monoprotic weak acid (α_1) goes to a maximum ($\alpha_1 = 1$) at some high pH and does not change at higher pH values. Hence, the plots of v_{eo} vs pH would be expected to become flat at high pH. The unexpected decrease in $|v_{eo}|$ suggests that anionic surface charge density decreases from pH 7.2 to 8.0. As discussed above, it is possible that adsorbed phosphate contributes to the surface charge on the carbon nanotubes. Perhaps at pH 8.0 adsorbed HPO_4^{2-} is displaced by OH^- resulting in a net decrease in the negative surface charge density.

The data in Figure 7A can be used to determine both the number density and pK_a of the surface acidic sites on the carbon nanotube membranes.[43] The Boltzmann equation is first used to calculate the surface hydronium ion concentration ($[H^+]_s$) from the bulk solution hydronium ion concentration ($[H^+]_o$).

$$[H^+]_s = [H^+]_o \exp(-e\zeta/2kT) \tag{11}$$

(44) Leon y Leon, C. A.; Solar, J. M.; Calemma, V.; Radovic, L. R. *Carbon* **1992**, *30*, 797−811.

The requisite ζ-potential values at each pH are obtained as before from the v_{eo} data (Figure 7A). Following Jimbo et al.,[43] the surface charge density is related to the number density of acidic sites (N_a) and the surface pK_a via

$$\sigma = -[(eN_a)/(1 + 10^{pK_a - pH_s})] \quad (12)$$

Equation 9 can be solved for σ and set equal to eq 12. Solving for the ζ-potential gives

$$\zeta = -[(eN_a)/(1 + 10^{pK_a - pH_s})](\kappa^{-1}/\epsilon) \quad (13)$$

Figure 7B shows a plot of ζ vs pH_s obtained from the data in Figure 7A, omitting the highest and lowest pH values where unusual effects (vide supra) were observed. The points are the experimental data; the curve is the result of a nonlinear least-squares regression fit of eq 13 to the experimental data using the surface pK_a and N_a as adjustable parameters. The best fit ($R^2 = 0.95$) was obtained for p$K_a = 4.7$ and $N_a = 0.03$ acidic sites per nm^2.

The surface pK_a value obtained is typical of that for an alkyl carboxylic acid (e.g., acetic acid) dissolved in aqueous solution. However, it is often the case that pK_a values for surface-bound species differ from those obtained when the corresponding molecule is dissolved in an aqueous solution. For example, the pK_a values for PABA[26] and 4-carboxyphenyl[45] immobilized on glassy carbon electrode surfaces were measured to be 3.0 and 2.8, respectively. These values are significantly different from the pK_a values for the same molecules dissolved in aqueous solution: PABA = 4.6 and benzoic acid = 4.2. For this reason, while the most likely assignment for the surface acidic sites is carboxylic acid, we cannot unambiguously make this assignment at this time. A less likely alternative would be to posit a surface phenolic site whose surface pK_a has been dramatically shifted from the typical solution value. One potential source for discrepancies between surface and free-solution pK_a values is electrostatic interactions between the surface-bound sites. The site density of 0.03 per nm^2 indicates that the sites are on average 3 nm apart.[46] This is comparable to the double-layer thickness at the ionic strength used to obtain the data in Figure 7. Hence, electrostatic interactions between surface acidic sites should not be significant.

The Effect of Electrochemical Derivatization on v_{eo}. An interesting advantage of the carbon nanotube membranes is that they are electronically conductive and thus can be used as electrodes in electrochemical experiments.[8,14,15] This has allowed us to electrochemically derivatize the carbon nanotube walls to augment or change the fixed surface charge.

Figure 8 shows a plot of v_{eo} vs applied current density for an as-synthesized carbon nanotube membrane and for membranes that had been electrochemically derivatized with either 2-(4-aminophenyl)ethylamine (APEA) or *p*-aminobenzoic acid (PABA).[26] The pH 7.2 buffer used was such that the carboxylic acid was deprotonated and the amine was protonated. Considering the as-synthesized membrane first, we see the expected (Table 1) change from positive electroosmotic flow at the positive applied current, to zero flow at no applied current, to negative EOF at negative applied current. The measured slope of the line corresponds to $\zeta = -20.8$ mV. The same trend is observed for the PABA-derivatized membrane, but the slope of the v_{eo} vs applied current density line is steeper and

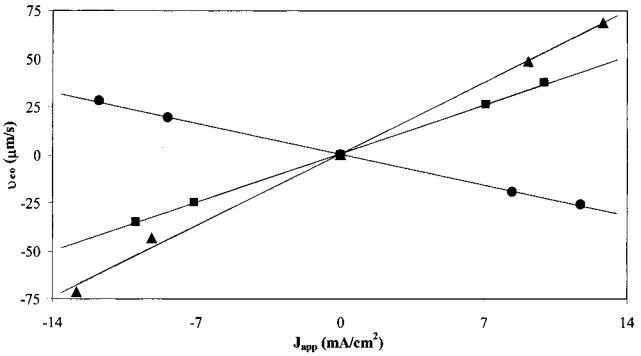

Figure 8. Plots of electroosmotic velocity vs applied current density for (▲) PABA-derivatized membrane, (■) as-synthesized membrane, and (●) APEA-derivatized membrane.

corresponds to $\zeta = -30.6$ mV. This indicates that there is greater negative surface charge density after attachment of PABA, which was the anticipated result.

For the AEPA-derivatized membrane, positive EOF is observed at negative applied currents and negative EOF is observed at positive applied currents (Figure 8). This indicates that the ζ-potential and thus surface charge is now positive, again the anticipated result. The ζ-potential for the AEPA-derivatized membrane was determined to be +13.2 mV. Note, however, that the magnitude of the ζ-potential for the AEPA-derivatized membrane is not as great as for either the underivatized or the PABA-derivatized membranes. While this might be due to a lower surface charge density for the AEPA-derivatized membrane, other factors contributing to ζ-potential (eq 8) must also be considered. For the as-synthesized and PABA-derivatized membranes, the solution-side of the double layer contains monovalent Na^+ ions. In contrast for the AEPA-derivatized membrane, the double layer contains a mixture of monovalent $H_2PO_4^-$ and divalent HPO_4^{2-} ions. The presence of the divalent ions (which are electrostatically preferred over the monovalent) will compress the double layer relative to the case where only monovalent ions are present.[47] As a result, at any surface charge density value, the double layer will be thinner when divalent ions are present. This will cause the ζ-potential to be lower and v_{eo} to be smaller than in the monovalent case. This factor undoubtedly contributes to the smaller slope for the AEPA-derivatized membrane (Figure 8).

Conclusions

EOF can be driven across template-prepared carbon nanotube membranes and the rate and direction of flow can be controlled by changing the magnitude and the sign of the transmembrane current. The direction of EOF can also be switched by varying the pH of the contacting solution phase, and all of the pH-induced changes in EOF are reversible. This means, for example, that returning a membrane that had been exposed to pH 3.5 buffer, where no EOF is observed (Figure 7A), to pH 7.2 buffer restored the flow. Electrochemical derivatization methods can be used to attach specific surface functional groups to the carbon nanotubes and this provides another route for adjusting the rate and direction of EOF.

There is a third possible way to affect the rate and direction of EOF in such membranes. We have shown with gold nanotube membranes that the sign and magnitude of the excess surface charge can be controlled potentiostatically by simply applying

(45) Saby, C.; Ortiz, B.; Champagne, G. Y.; Belanger, D. *Langmuir* **1997**, *13*, 6805−6813.

(46) Cheng, I. F.; Whiteley, L. D.; Martin, C. R. *Anal. Chem.* **1989**, *61*, 762−766.

(47) Burns, D. B.; Zydney, A. L. *J. Membr. Sci.* **2000**, *172*, 39−48.

a potential to the membrane in an electrolyte solution.[48] When negative potentials are applied, the nanotubes have excess negative (electron) surface charge and when positive potentials are applied the nanotubes have excess positive surface charge. This ability to control excess surface charge potentiostatically is unique to membranes that are electronically conductive, as are the Au and carbon nanotube membranes. We are currently investigating whether this simple potentiostatic charging method can be used to control EOF in the carbon nanotube membranes.

(48) Nishizawa, M.; Menon, V. P.; Martin, C. R. *Science* **1995**, *268*, 700−702.

Acknowledgment. Aspects of this work were supported by the National Science Foundation and the Office of Naval Research. The authors acknowledge valuable discussions with Prof. Henry White and Prof. Richard McCreery and thank David Mitchell for assistance with SEM analysis.

JA011926P